Atmospheric and Climate Sciences, 2025, 15(2), 476-494
https://www.scirp.org/journal/acs
ISSN Online: 2160-0422
ISSN Print: 2160-0414

Sharp Increase in June to August Minimum Temperature in 2013 over Rwanda: Assessment of Possible Potential Causes and Related Changes in Atmospheric Circulation Patterns

Jean Paul Kalisa[1], Guirong Tan[1*], Jonah Kazora[1,2], Conteh Moneh[1], Gerverse Kamukama Ebaju[3]

[1]School of Atmospheric Science, Nanjing University of Information Science and Technology, Nanjing, China
[2]Rwanda Meteorology Agency (Meteo Rwanda), Kigali, Rwanda
[3]School of Ecology and Applied Meteorology, Nanjing University of Information Science and Technology, Nanjing, China
Email: *tanguirong@nuist.edu.cn

How to cite this paper: Kalisa, J.P., Tan, G.R., Kazora, J., Moneh, C. and Ebaju, G.K. (2025) Sharp Increase in June to August Minimum Temperature in 2013 over Rwanda: Assessment of Possible Potential Causes and Related Changes in Atmospheric Circulation Patterns. *Atmospheric and Climate Sciences*, **15**, 476-494.
https://doi.org/10.4236/acs.2025.152025

Received: February 28, 2025
Accepted: April 21, 2025
Published: April 24, 2025

Abstract

Rwanda, a landlocked agricultural country, experienced escalating climate risks since 2013 due to rising June to August (JJA) minimum temperatures (Tmin), harming farming zones, lowering yields, risking health, and threatening economy. This study examined drivers of Rwanda's 2013 warming anomaly that severely affected eastern/central lowlands, analyzing circulation changes (1983-2021) using multiple datasets including Enhancing National Climate Services for Rwanda (ENACTS-Rwanda), European Centre for Medium-Range Weather Forecasts Reanalysis 5th Generation (ERA5), and National Oceanic and Atmospheric Administration (NOAA) observations. Methodologies included Empirical Orthogonal Function (EOF) decomposition, Mann-Kendall trend tests, Sen's slope estimator, and composite analysis to quantify trends and atmospheric linkages. Results showed a significant post-2013 Tmin increase (+0.4˚C to +2.1˚C) exceeding maximum temperature (Tmax) trends. EOF analysis identified a dominant warming mode (72% variance, loadings to +0.872) linked to coupled processes such as increased vertical descending, increased 850-hPa specific humidity, increased low-level cloud cover, but reduced precipitation, which collectively promoted nighttime warming through warm advection. The anomaly was amplified by El Niño-Southern Oscillation (ENSO)-induced Pacific warming and enhanced East African moisture transport. These findings demonstrated how local thermodynamic processes interacted with global climate, forcing them to produce extreme Tmin conditions. The results suggested adaptive strategies, including heat-resistant crop cultivation and optimized water management, could mitigate agricultural impacts. Future research should incorporate these mechanisms into regional climate models while quantifying non-meteorological contributions to observed warming trends, providing critical insights for climate resilience planning in Rwanda and similar regions.

Keywords

Climate Variability, Temperature Extremes, Atmospheric Circulation Patterns, Rwanda, June-July-August (JJA)

1. Introduction

Global warming has emerged as a critical global issue, driven by both human activities and natural processes. Temperature, more than any other meteorological parameter, plays a crucial role in detecting and assessing the climatic changes caused by urbanization and industrialization [1]. The significant increase in Earth's temperatures has profoundly altered the global climate system, resulting in notable climate changes across various temporal and spatial scales [2]. Human activities, primarily through greenhouse gas emissions, have caused global warming, with global surface temperatures reaching 1.1˚C above 1850 - 1900 levels during 2011-2020. The rate of temperature increase since 1970 has been the fastest in any 50-year period in at least the last 2000 years [3].

Projections indicate that the Global warming trend will continue, with temperatures expected to increase by an average of 1.5˚C by the 2030s [4]. The inconsistency in temperature patterns has prompted studies aimed at evaluating the variations in both the Tmax and Tmin [5]. Temperature extremes, particularly the increasing rate of Tmin, have garnered significant attention in climate studies. Monthly averages of Tmax and Tmin across more than 50% of the Northern Hemisphere and 10% of the Southern Hemisphere land area, which together comprise 37% of the global landmass, show that the increase in Tmin has occurred at a rate three times faster than that of Tmax between 1951 and 1990 [6].

Rwanda's Tmin is anticipated to rise from around 1.0˚C in 2021 to 2.5˚C by 2100 under the RCP 4.5 W/m^2 scenario. In the Musanze district, under the RCP8.5 scenario, the average annual Tmax and Tmin for 2071-2100 are expected to rise by 4.3˚C and 3.8˚C, respectively, relative to the 2006-2035 baseline. These forecasts are consistent with research highlighting that Rwanda's temperature increase will exceed the global average [7] [8]. Research revealed that Rwanda has experienced a notable warming trend over the last century, with average temperature increases ranging from 0.7˚C to 0.9˚C, displaying regional and seasonal variations [9] [10]. The spatial patterns of Tmax and Tmin demonstrate a clear warming trend across the entire country, particularly since the early 1980s. Tmax trends show substantial increases in all regions, with rates ranging from 0.40˚C to 0.49˚C per decade at different elevations [5]. Notable positive trends in Tmin were observed, especially during the long dry season and short rainy season, with average increases of 0.17˚C and 0.20˚C per decade, respectively. The occurrence of warm days and nights has grown, with warm days increasing by 1.28 days per decade. Tmax exhibits greater variability than Tmin, especially in the eastern and north-western highlands [4].

Although warming trends are well-documented, a notable research gap persists in understanding the atmospheric mechanisms propelling extreme temperature events, such as the pronounced JJA Tmin escalation in Rwanda in 2013 and their linkage to long-term atmospheric circulation patterns. Previous investigations have identified widespread increases Tmax and Tmin across Rwanda, yet the specific drivers of the 2013 JJA Tmin anomaly—particularly in the more susceptible eastern and central lowlands-remain insufficiently examined. This study addresses this deficiency by exploring the 2013 JJA Tmin surge, which exhibited sustained intensification through 2021, across Rwanda, a landlocked East African nation where agriculture forms a cornerstone of the economy. The analysis spans atmospheric circulation dynamics from 1983 to 2021, employing trend analysis, Empirical Orthogonal Function (EOF) techniques, and composite methods to unravel temperature variability, detect pivotal shifts, and evaluate influences from large-scale climate systems. Alterations in vertical motion, equatorward winds, velocity potential, water vapor transport, relative humidity, and cloud cover were scrutinized, demonstrating how reduced cloudiness, enhanced moisture flux, and modified wind regimes amplified nighttime warming. Local processes interacted with global phenomena, notably the ENSO, which intensified the anomaly through heightened Pacific warming and East African convective activity post-2013.

These findings illuminate the atmospheric and global factors driving Rwanda's temperature extremes, with the eastern and central lowlands emerging as critical zones of sensitivity. This deepened insight into climate variability informs the development of targeted adaptation strategies to safeguard agriculture, water resources, and socio-economic stability in climate-vulnerable regions. Furthermore, the study enhances climate modeling and risk management approaches for future temperature extremes, while emphasizing the necessity of continued research to refine predictive tools and disentangle the complex interplay of local and global climatic forces.

2. Data and Methodology

2.1. Study Area

Rwanda, a landlocked country in East Africa, is located between latitudes 1˚S and 3˚S and longitudes 28˚E and 31˚E, bordered by Tanzania, the Democratic Republic of Congo, Uganda, and Burundi (**Figure 1**). Rwanda experiences two main rainy seasons, March to May (MAM) and September to December (SOND), and two main dry seasons: the long dry season (JJA) and a short dry season from January to February (JF). These alternating dry and wet seasons are due to the passage of the Intertropical Convergence Zone (ITCZ) through the region, with the dry periods marked by reduced rainfall and increased temperatures, making them critical for understanding the impacts of climate variability. The country's diverse topography is divided into four physiographic regions: the Lake Kivu area, the Nile-Congo divide, the plateau region, and the eastern lowlands. The eastern lowlands are the driest and warmest, while the mountainous Nile-Congo divide, which includes the Virunga Mountains and Nyungwe forest, is the wettest and coolest region. The Lake Kivu and plateau regions fall between these extremes, showing intermediate levels of temperature, precipitation, and elevation. Given the importance of these climatic variations, especially during the dry seasons, Rwanda's distinct geography and seasonal shifts make it a critical area for studying the impacts of temperature extremes and the mechanisms driving climatic changes, particularly in relation to atmospheric circulation patterns.

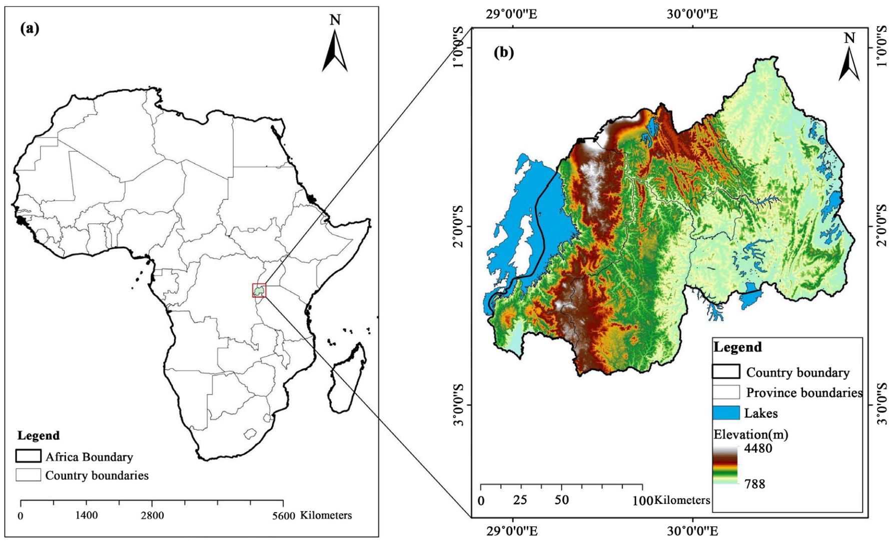

Figure 1. The study area: (a) Map of Africa; (b) Elevation map of Rwanda.

2.2. Temperature Climatology of Rwanda

Rwanda's climate is characterized by a temperate tropical highland climate, with mean annual temperatures averaging around 19.1˚C. This stability is influenced by the country's varied topography, leading to notable spatial variations in temperature. Regions below 1500 meters, such as the Eastern Province, experience annual temperatures exceeding 20˚C. Areas between 1500 and 3000 meters maintain temperatures ranging from 15˚C to 20˚C. The Virunga Mountains, with elevations above 3000 meters, record temperatures below 15˚C [11]. Recent analyses indicate a significant warming trend, with maximum temperatures increasing at rates of 0.40˚C to 0.49˚C per decade across various regions [7]. The highest Tmax and Tmin occur in the lowlands during the JJA and January to February (JF) dry seasons [12] [13]. Tmax and Tmin decrease gradually with topography from east to west in all seasons. Warmest annual average temperatures are found in the eastern plateau (20˚C - 21˚C) and south-eastern valley of Rusizi (23˚C - 24˚C) in the south-west, and cooler temperatures are found in higher elevations of the central plateau (17.5˚C - 19˚C) and high lands (<17˚C) in the north and north-west [11]. For instance, the rise in average temperatures is projected to increase the number of hot days and nights by 12% - 58% and 31% - 86%, respectively [7].

2.3. Data Source

2.3.1. ENACTS Dataset

The Enhancing National Climate Services (ENACTS) dataset is integral to understanding temperature variations in Rwanda. By integrating station observations with satellite data and temperature reanalysis, this dataset addresses historical data gaps and provides high-resolution climate data essential for analyzing temperature extremes. With a spatial resolution of 4 to 5 km, it enables detailed analysis of temperature variations across Rwanda's diverse topographies [14]. Datasets like ENACTS are crucial due to Rwanda's vulnerability to climate change, informing policy and adaptation strategies, particularly concerning increasing temperature variability and its effects on agriculture and water resources [4].

2.3.2. ERA5 Data from the Copernicus Climate Data Store (CDS)

The analysis of Rwanda's climate patterns, especially regarding temperature extremes, is significantly improved by incorporating ERA5 data from the Copernicus Climate Data Store. This high-resolution global reanalysis dataset offers key atmospheric variables that enable a thorough understanding of both short-term fluctuations and long-term trends in temperature variability. ERA5 provides data on temperature, pressure, wind speed, humidity, etc., which are essential for studying atmospheric circulation patterns. With data spanning from 1950 to the present, ERA5 establishes a robust temporal foundation for climate analysis [15]. Combining ERA5 with ENACTS allows a detailed examination of Rwanda's climate extremes.

2.3.3. National Oceanic and Atmospheric Administration (NOAA)

NOAA's climate datasets, such as the U.S. Climate Extremes Index (CEI) and the Global Historical Climatology Network (GHCN), offer crucial context that helps in analyzing temperature extremes in Rwanda. These datasets, along with NOAA's reanalysis products (e.g., NCEP/NCAR Reanalysis and ERA5), support the identification of atmospheric circulation anomalies that may influence temperature shifts in Rwanda. The CEI offers insights into extreme weather events, aiding in the assessment of temperature anomalies in Rwanda, while the GHCN provides essential historical temperature data to analyze long-term trends. NOAA's reanalysis tools help correlate atmospheric circulation anomalies with temperature variations and its climate models project future warming trends [16].

2.4. Methodology

2.4.1. The Mann-Kendall (MK) Test

The MK test is a non-parametric method resistant to outliers and is used to detect monotonic trends in data. It calculates the statistic S based on the differences between later and earlier values (Equation (1)); a large positive S indicates an increasing trend, while a large negative S indicates a decreasing trend [17] [18]. The variance of S is computed considering tied groups, and the significance of the trend is determined by the Z score. A significant trend is identified when the Z value exceeds confidence limits [19] [20].

$$S = \sum_{i=0}^{n-1} \sum_{j=i+1}^{n} sign\left(Y_j - Y_i\right) \tag{1}$$

where (Y_j, Y_i) is equal to +1, 0, or −1.

$$Sign\left(Y_j - Y_i\right) = \begin{cases} 1 & \text{if } Y_j - Y_i > 0 \quad (1\text{-}1) \\ 0 & \text{if } Y_j - Y_i = 0 \quad (1\text{-}2) \\ -1 & \text{if } Y_j - Y_i < 0 \quad (1\text{-}3) \end{cases}$$

$\left(Y_j - Y_i\right)$, where $j > 1$, and assign the integer 1, 0 or −1 to positive difference, no difference, and negative differences, respectively.

The variance of S was calculated using Equation (2) as follows:

$$Var\left(S\right) = \frac{n\left(n-1\right)\left(2n+5\right) - \sum_{i=1}^{p} t_i\left(t_i - 1\right)\left(2t_i + 5\right)}{18} \tag{2}$$

n: the number of data points, p: the number of tied groups, and t_i: the number of data values in the p^{th} group.

The significance of the trend is computed by Z score with Equation (3) as follows:

$$Z = \frac{S-1}{\sqrt{Var\left(S\right)}} \text{ if } S > 0,\ Z = 0 \text{ if } S = 0, \text{ and } Z = \frac{S+1}{\sqrt{Var\left(S\right)}} \text{ if } S < 0. \tag{3}$$

2.4.2. The Sen's Slope Estimator

It's a non-parametric method used to quantify the magnitude of trends in time series data. It is commonly applied to detect seasonal temperature trends and serves as an alternative to linear regression for estimating trend slopes. If a linear trend is present, the true slope is determined using the Sen-Theil trend line [21]. This estimator is often used alongside the Mann-Kendall test to assess trend significance. The slope (T_i) between two random values in each time series is computed using the Equation (4) as follows

$$T_i = \frac{X_j - X_k}{j - k} \text{ for } i = 1,2,3,\cdots,N \tag{4}$$

x_j and x_k are data values at time j and k, respectively, $\left(j > k\right)$. The median of these N values of T_i is represented as Sen's estimator of the slope:

$$Q_i = \begin{cases} T_{\frac{N+1}{2}} & N \text{ is odd} \\ 1/2\left(T_{\frac{N}{2}} + T_{\frac{N+2}{2}}\right) & N \text{ is Even} \end{cases} \tag{5}$$

Sen's estimator is computed as $Q_{med} = T_{(N+1)/2}$ if N appears odd, and it is considered as $Q_{med} = T_{\frac{N}{2}} + T_{\frac{N+2}{2}}$ if N appears even. Finally, Q_{med} is calculated by a two-sided test at $100(1-\alpha)\%$ the confident interval, which in turn helps to get the true slope through the non-parametric test. A positive value of Q_i indicates an increasing trend and a negative value of Q_i gives a decreasing trend in time series.

2.4.3. Empirical Orthogonal Function (EOF)

EOF is a statistical method that performs matrix computations, yielding eigenvectors and eigenvalues that capture both spatial and temporal variability. This technique identifies spatial patterns of variability (EOFs) and their associated temporal fluctuations (Principal Components or PCs), providing an amplitude of variability across different timescales [22]. The first EOF corresponds to the largest eigenvalue of the covariance matrix, reflecting the greatest variance, while the second EOF represents the second-largest eigenvalue. The first (PC1) represents the magnitude of the eigenvalue in the time series and is associated with the first EOF (EOF1), while PC2 corresponds to EOF2 [23]. This kind of analysis has been employed to reveal dominant temperature patterns during JJA, highlighting periods of high variability. Furthermore, based on the dominant mode identified through EOF, the composite analysis method has been applied to examine atmospheric circulation systems that contribute to temperature variability during JJA season in Rwanda.

3. Results and Discussion

3.1. Variation of JJA Tmax and Tmin

The analysis of JJA temperature variations in Rwanda from 1983 to 2021 revealed distinct differences between Tmax and Tmin, with a notable and sustained spike in JJA Tmin beginning in 2013. Spatially, Tmax ranged from 22.0˚C to over 30.6˚C, with warmer conditions in the Eastern and Southern lowlands and cooler temperatures in the Western and Northern highlands, showing temporal stability (**Figure 2(a)**). Tmin ranged from 9.7˚C to over 17.2˚C, with warmer eastern lowlands suggesting nighttime warming tied to the persistent 2013-2021 anomaly (**Figure 2(b)**). Temporally, Tmax remained stable (24.5˚C - 25.5˚C) with a slight upward trend (**Figure 2(d)**), while Tmin exhibited a sharp rise after the early 2000s, peaking above 15.5˚C in 2013-2014—well above the long-term average of approximately 14.5˚C—and continued to increase through 2021 (**Figure 2(c)**). This sustained spike was underscored by Tmin anomalies, which showed a marked positive deviation exceeding +1.5˚C from 2013-2014 onward (**Figure 2(e)**), whereas Tmax anomalies remained minor and stable, fluctuating within ±1˚C (**Figure 2(f)**).

The prolonged Tmin increase likely stemed from shifts in atmospheric circulation, including altered wind patterns, elevated humidity, and large-scale influences like ENSO, potentially reducing nighttime cooling and increasing water vapor in lowland areas. This indicated a significant climatic shift starting in 2013, driven by local and global dynamics, with critical implications for understanding Rwanda's temperature extremes and guiding climate adaptation strategies.

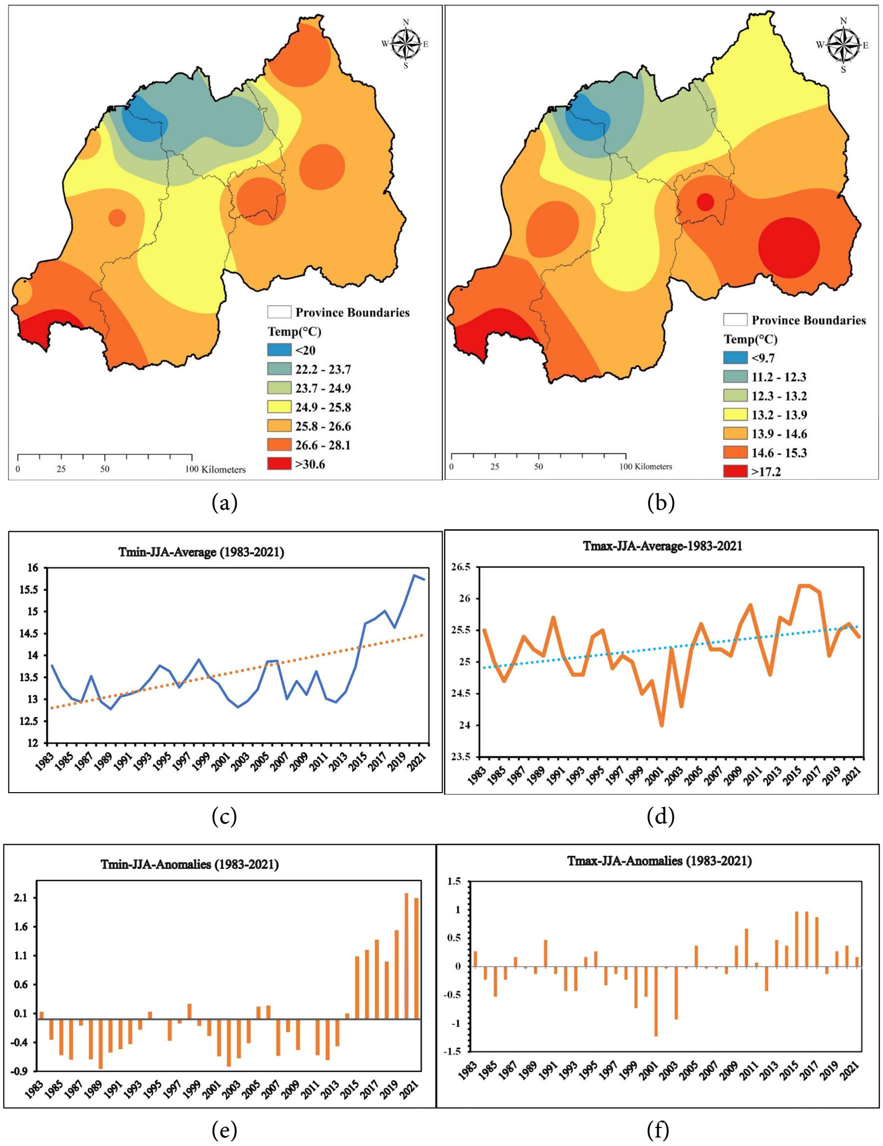

Figure 2. June to August (JJA) temperature patterns, 1983-2021. (a) Spatial average of Tmax; (b) Spatial average of Tmin; (c) Temporal average of Tmin; (d) Temporal average of Tmax; (e) Tmin anomalies; (f) Tmax anomalies.

3.2. Leading EOF Modes for Both Tmax and Tmin

The EOF analysis of JJA temperature variability in Rwanda from 1983 to 2021 revealed distinct patterns for Tmax and Tmin, with significant insights into the sharp increase in JJA Tmin in 2013. PC1 of Tmax showed stable variability, fluctuating around zero with values ranging from −30% to +20% and no notable trend or spike, which indicated that Tmax remained relatively consistent over time (**Figure 3(a)**). In contrast, PC1 of Tmin, exhibited a pronounced upward trend, particularly around 2013-2014, with values rising sharply to over +30%, directly aligning with the observed anomaly in Tmin. This spike, sustained post-2013, underscored a dominant mode of Tmin variability tied to a significant climatic event (**Figure 3(b)**). Spatially, the EOF1 pattern for Tmax showed balanced variability, with positive values (0.672 - 0.881) in the central and eastern regions and negative values (−0.881 - (−0.065)) in the western and northern highlands, reflecting a stable distribution (**Figure 3(c)**). For Tmin, the EOF1 pattern highlighted strong positive values (0.606 - 0.849) in the eastern and southern lowlands, indicating these areas contributed most to the 2013 Tmin increase, while negative values (−0.849 - (−0.065)) appear in the highlands (**Figure 3(d)**). These findings suggested that the 2013 anomaly was driven by atmospheric circulation changes, such as altered wind patterns, humidity, or large-scale drivers like ENSO, particularly affecting nighttime warming in lowland regions, with no similar impact on Tmax. This analysis highlighted the interplay between local and global climatic forces, providing critical insights into Rwanda's temperature extremes and informing climate adaptation strategies.

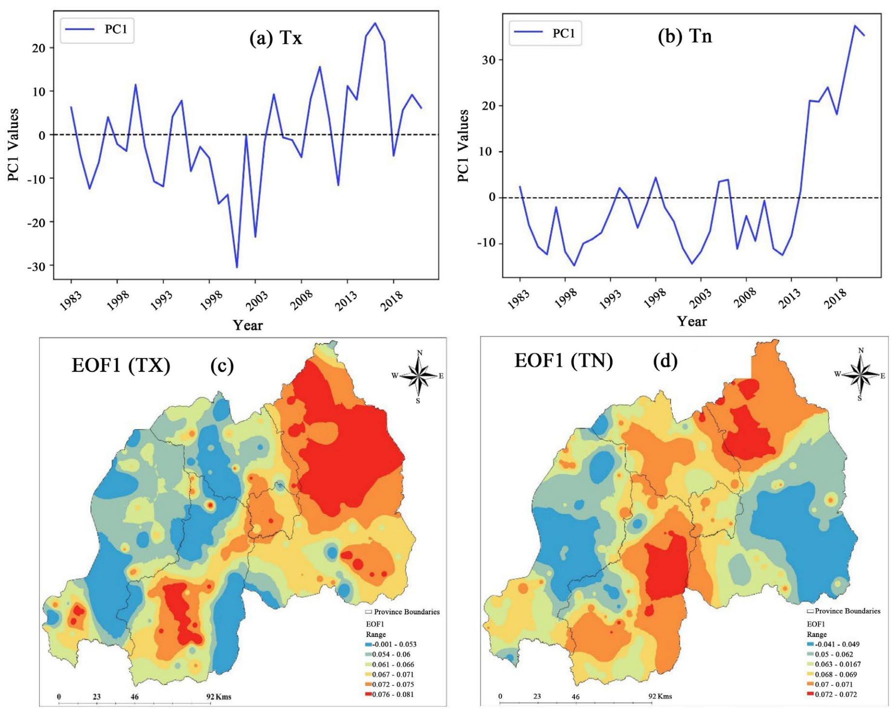

Figure 3. Leading modes of June to August (JJA) temperature variability, 1983-2021. (a) PC1 of Tmax; (b) PC1 of Tmin; (c) EOF1 of Tmax; (d) EOF1 of Tmin.

3.3. Dynamics of JJA Tmin Variability in Rwanda: Insights into the 2013-2014 Anomaly

The EOF analysis of JJA Tmin in Rwanda from 1983 to 2021, detailed in **Figure 4**, provided comprehensive insights into regional variability and revealed a significant warming trend, particularly evident around the sharp increase in JJA Tmin in 2013. The central map displayed the spatial pattern of the first EOF mode

(EOF1) for Tmin, with values ranging from −0.872 to +0.872, highlighting dominant modes of variability across the country. Red areas (positive values, 0.606 - 0.872) were concentrated in the eastern and southern regions, such as Kigoma and Kiziguro, indicating these lowland areas experienced the strongest positive variability in Tmin, contributing to the 2013 anomaly. Blue areas (negative values, −0.872 - (−0.065)) were found in the western and northern highlands, showing opposite variability trends. Accompanying time series for specific stations, Kigoma (South, Figure 4(a)) and Kiziguro (East, Figure 4(b)), further illustrated this pattern, with Kigoma's Tmin rising from about 13˚C in the 1980s to 16.5˚C by the early 2020s and Kiziguro's Tmin increasing from 13.5˚C to 15.5˚C, over the same period, both showing a notable upward trend and a sharp spike around 2013-2014, aligning with the national anomaly. Figure 4(c) shows stable Tmin anomalies (1983-2013) fluctuating around zero (−0.9˚C to +0.3˚C), while Figure 4(d) revealed a clear rise in anomalies (2014-2021) from −0.1˚C to +2.4˚C, indicating sustained warming post-2013. Post-2013, Tmin values in these regions remained elevated, suggesting a persistent warming effect, particularly in the central lowlands. These spatial and temporal patterns, consistent with Figure 3(c) highlighting warmer areas (red and orange) and cooler areas (blue and green), indicated that the 2013 Tmin increase was most pronounced in eastern and southern lowlands, likely driven by changes in atmospheric circulation, such as altered wind patterns, humidity, or large-scale drivers like ENSO, which amplified nighttime warming in these areas. This analysis underscored a widespread warming trend in Rwanda's central lowlands after 2013, reinforcing the role of regional climatic dynamics in explaining the country's temperature extremes and supporting the need for targeted climate adaptation strategies.

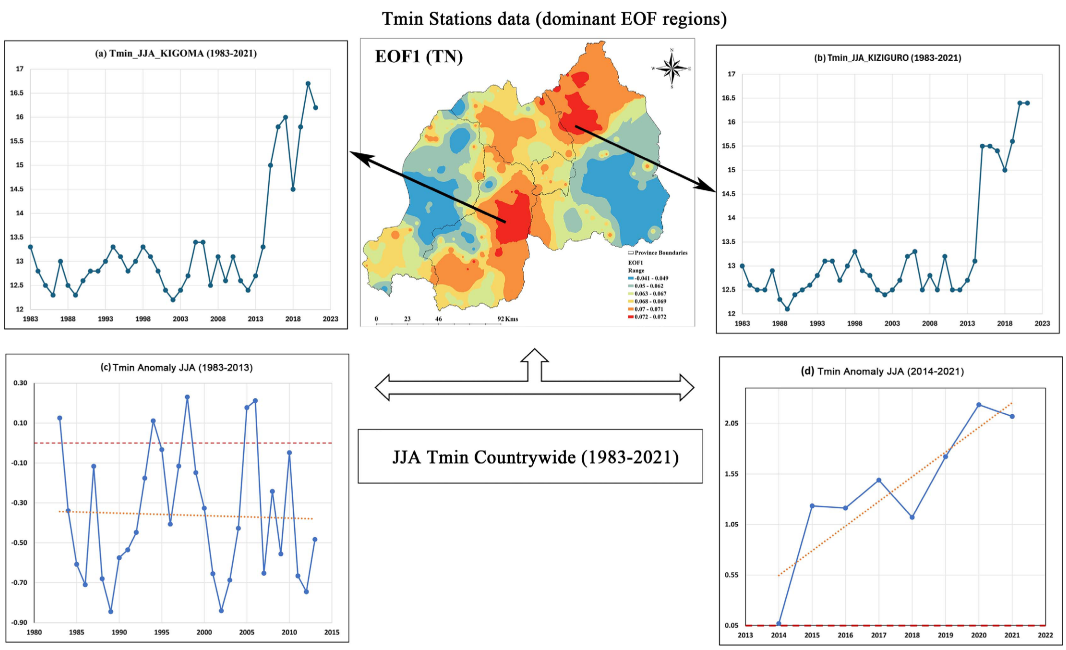

Figure 4. JJA Tmin at localized stations in leading EOF regions, 1983-2021. (a) Kigoma station; (b) Kiziguro station; (c) Anomaly Tmin over Rwanda, 1983-2013; (d) Anomaly Tmin over Rwanda, 2014-2021.

3.4. Atmospheric Circulation Analysis of Tmin Sharp Increase Near 2013

3.4.1. Effects of Vertical Motion, Moisture Transport and Rainfall

The atmospheric circulation analysis, focusing on the sharp increase in Rwanda's JJA Tmin around 2013, revealed key climate factors driving this change across the region, with specific impacts on Rwanda, as shown in **Figure 5**. Vertical cross-sections of vertical motion and equatorward winds over the region, depicted in **Figures 5(a)-(c)**, highlighted significant shifts between 1983-2013 and 2014-2021.

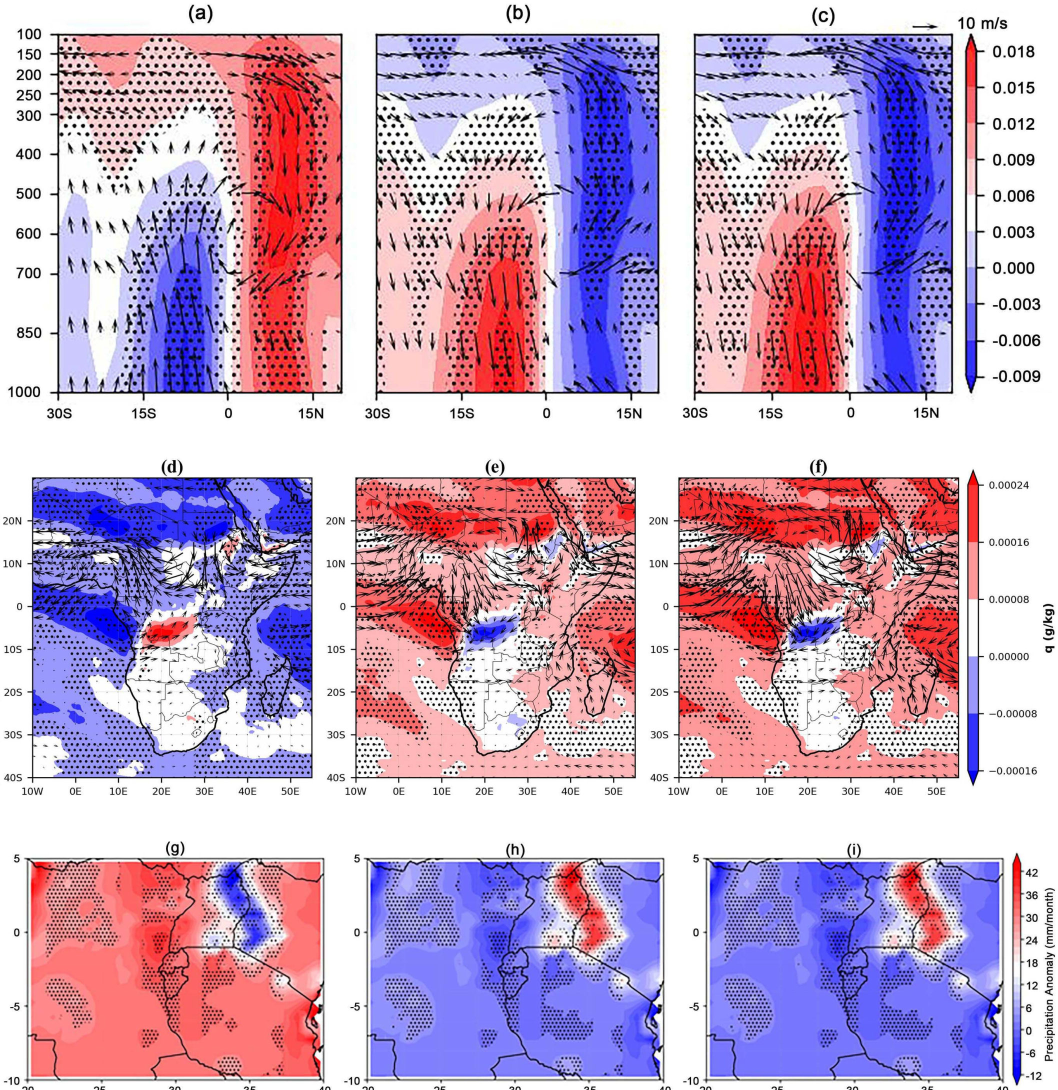

Figure 5. Vertical Motion (shadings, Pa/s), equatorward winds (vectors, m/s), specific humidity (shadings, g/kg), moisture transport (vectors, g/kg·m/s), and rainfall (shadings, mm/month), with 95% Confidence level indicated by dots representing statistical significance. (a) Vertical Motion and equatorward winds for 1983-2013; (b) Vertical Motion and equatorward winds for 2014-2021; (c) Difference in Vertical Motion (and equatorward winds between 2014-2021 and 1983-2013; (d) Specific humidity and moisture transport for 1983-2013; (e) Specific humidity and moisture transport for 2014-2021; (f) Difference in specific humidity and moisture transport between 2014-2021 and 1983-2013; (g) Rainfall for 1983-2013; (h) Rainfall for 2014-2021; (i) Difference in rainfall between 2014-2021 and 1983-2013.

During 1983-2013, Figure 5(a) showed stable conditions in the region with moderate upward motion and southerly winds up to 20 m/s, while Rwanda experienced neutral vertical motion and typical wind patterns. By 2014-2021, Figure 5(b) indicated stronger upward motion (+0.012 Pa/s) and intensified southerly winds (up to 25 m/s) across the region, with Rwanda's eastern and central lowlands showing enhanced ascent, suggesting increased vertical motion and moisture transport. The difference in Figure 5(c) confirmed a post-2013 increase in these factors, likely reducing nighttime cooling and contributing to Rwanda's Tmin spike.

The specific humidity in the region was moderate from 1983-2013 (Figure 5(d)), rising to higher levels in Rwanda's eastern and central lowlands by 2014-2021 (Figure 5(e)), with a significant increase post-2013 (Figure 5(f)), likely trapping more heat at night. Rainfall across the region decreased slightly in 1983-2013 (Figure 5(g)), dropping more noticeably in 2014-2021 (Figure 5(h)), with Rwanda's eastern lowlands showing a pronounced drying trend by 2015 (Figure 5(i)). These findings indicated that the 2013 Tmin increase in Rwanda resulted from enhanced upward motion, stronger winds, higher humidity, and reduced rainfall, reflecting altered atmospheric circulation across the region where Rwanda is located, likely influenced by large-scale drivers like ENSO, which led to less cooling and greater heat retention, particularly Eastern and Central lowlands.

3.4.2. Velocity Potential Influences

The analysis of velocity potential at 200 hPa and 850 hPa across the global tropics during JJA, as depicted in Figure 6, provides critical insights into atmospheric circulation shifts that contributed to Rwanda's pronounced JJA Tmin escalation in 2013, with effects spanning global, regional, and local scales. At the upper level (200 hPa), Figure 6(a) (1983-2013) showed a global pattern of strong divergence (red) over the central Pacific and convergence (blue) over the western Pacific and Africa, with wind vectors indicating upper-level divergence over East Africa. Figure 6(b) (2014-2021) revealed a shift, with convergence (blue) over the eastern Pacific and enhanced divergence (red) over Africa, particularly East Africa, suggesting intensified upper-level divergence. The difference (Figure 6(c)) highlighted stronger convergence over the central Pacific and increased divergence over East Africa post-2013, reinforcing this pattern. Regionally, this shift indicated heightened upper-level divergence over East Africa, promoting convection. In Rwanda, this enhanced divergence likely contributed to reduced cloud cover and increased radiative heating, elevating Tmin.

At the lower level (850 hPa), Figure 6(d) (1983-2013) depicted global convergence (blue) over the western Pacific and divergence (red) over the eastern Pacific and parts of Africa, with winds indicating upward motion over Rwanda. Figure 6(e) (2014-2021) showed strengthened convergence (blue) over the central Pacific and increased divergence (red) over East Africa, with wind patterns reinforcing upward motion over Rwanda. The difference (Figure 6(f)) confirmed more pronounced divergence over East Africa and stronger convergence in the central Pacific post-2013, amplifying these changes. Regionally, this intensified low-level divergence over East Africa enhanced moisture transport and convection, reducing cloud cover. In Rwanda, particularly in the eastern and central lowlands, this amplified upward motion likely diminished low-level, high-level, and total cloud cover, reducing nighttime cooling and driving the sustained Tmin rise through 2021.

These shifts suggested a strengthened Walker Circulation, likely driven by a significant El Niño event, which enhanced upward motion, moisture transport, and convection over East Africa. This alteration in large-scale atmospheric circulation reduced nighttime cooling in Rwanda by increasing radiative heating, contributing to the 2013 Tmin spike and demonstrating how global circulation patterns influence local temperature extremes in Rwanda, particularly in the vulnerable eastern and central lowlands, underscoring the need for targeted climate adaptation strategies.

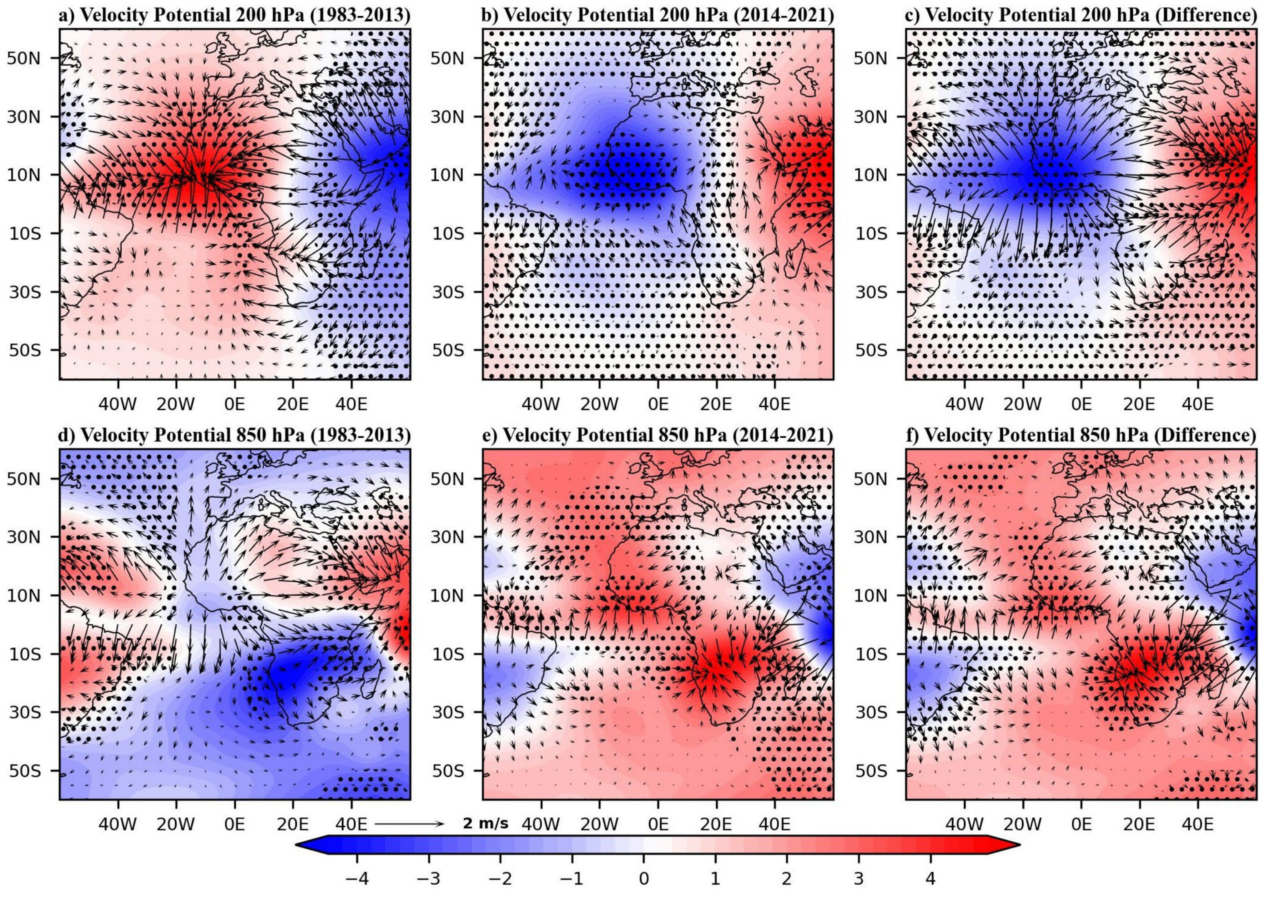

Figure 6. Velocity potential hPa (shadings, m^2/s^2) at 200 hPa and 850 hPa over the global tropics during JJA, with 95% Confidence Interval indicated by dots representing statistical significance. (a) Velocity potential at 200 for 1983-2013; (b) Velocity potential at 200 hPa for 2014-2021; (c) Difference in velocity potential at 200 hPa between 2014-2021 and 1983-2013; (d) Velocity potential at 850 hPa for 1983-2013; (e) Velocity potential at 850 hPa for 2014-2021; (f) Difference in velocity potential at 850 hPa between 2014-2021 and 1983-2013.

3.5. Cloud Cover Anomalies and Their Role in the 2013 JJA Tmin Escalation in Rwanda

This investigation examined the 2013 JJA Tmin spike in Rwanda and its atmospheric circulation drivers from 1983 to 2021, analyzing cloud cover anomalies across East Africa with a focus on Rwanda, as shown in **Figure 7**. The figure presented low-level cloud (LLC), mid-level cloud (MCC), high-level cloud (HCC), and total cloud cover (TCC) anomalies for 1983-2013 and 2014-2021, with difference maps highlighting shifts and dots indicating statistical significance at a 95% confidence level. This analysis aligned with the research objectives of quantifying the 2013 anomaly, evaluating Tmin trends, and assessing atmospheric and global influences, particularly in Rwanda's eastern and central lowlands.

During 1983-2013, cloud cover anomalies across East Africa, including Rwanda, displayed moderate variability: LLC (**Figure 7(a)**) anomalies ranged from −10% to +4.8%, with Rwanda showing slight positive anomalies (up to +2%) in the west and near-neutral conditions in the east; MCC (**Figure 7(d)**) anomalies varied from −12% to +16%, with Rwanda exhibiting slight positive anomalies (up to +4%) centrally but negative anomalies (−4%) in the east; HCC (**Figure 7(g)**) anomalies spanned −6% to +18%, with Rwanda displaying positive anomalies (up to +6%) in the west and near-neutral conditions in the east; TCC (**Figure 7(j)**) anomalies ranged from −8% to +24%, with Rwanda showing slight positive anomalies (up to +4%) across most regions, indicating a balanced radiative environment.

From 2014 to 2021, significant cloud cover shifts emerged in Rwanda: LLC (**Figure 7(b)**) anomalies decreased sharply, ranging from −17.5% to +2.5%, with the eastern and central lowlands experiencing a pronounced decline (up to −15%) and the west a smaller reduction (−5%); MCC (**Figure 7(e)**) anomalies ranged from −4.5% to +6%, with an increase (up to +4%) in the east but a decrease (−4%) in the west; HCC (**Figure 7(h)**) anomalies shifted from −7.5% to +3%, with a decline (up to −4%) in the east and central regions; TCC (**Figure 7(k)**) anomalies ranged from −7.5% to +3%, with a significant reduction (up to −6%) in the eastern and central lowlands.

The difference maps underscored these changes: LLC (**Figure 7(c)**) anomalies ranged from −24% to +3%, with Rwanda's eastern and central lowlands showing the largest decline (up to −18%); MCC (**Figure 7(f)**) anomalies varied from −6% to +8%, with the east displaying a slight increase (+2%); HCC (**Figure 7(i)**) anomalies spanned −9% to +3%, with a decline (up to −5%) in the east and central regions; TCC (**Figure 7(l)**) anomalies ranged from −12% to +4%, with a significant reduction (up to −8%) in the eastern and central lowlands. Dynamical processes analysis indicated that the post-2013 reduction in LLC, HCC, and TCC enhanced downward longwave radiation and elevated Tmin by reducing nighttime cooling, while the MCC increase in the east influenced local convection. These shifts, potentially driven by ENSO-induced Pacific warming, highlighted the eastern and central lowlands' vulnerability to Tmin extremes.

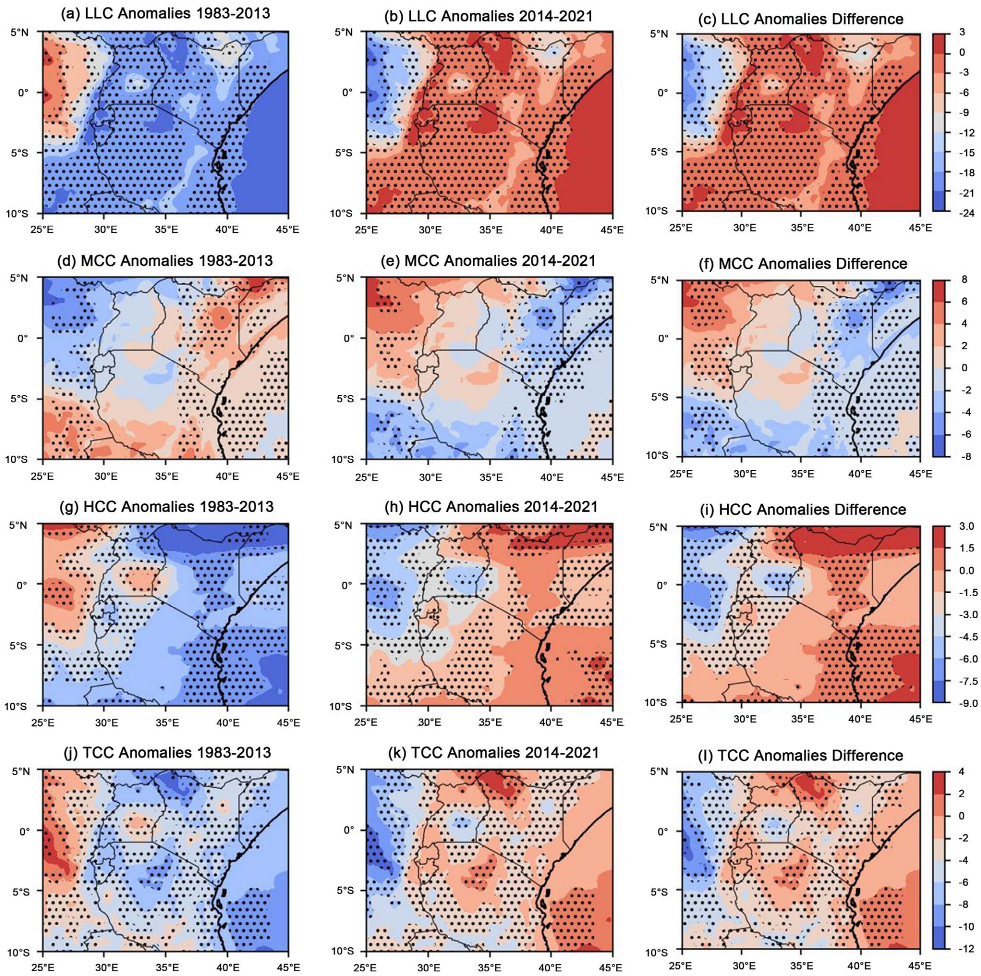

Figure 7. Cloud cover anomalies during JJA, with 95% Confidence Interval indicated by dots representing statistical significance. (a) Low-level clouds for 1983-2013; (b) Low-level clouds for 2014-2021; (c) Difference in low-level clouds between 2014-2021 and 1983-2013; (d) Mid-level clouds for 1983-2013; (e) Mid-level clouds for 2014-2021; (f) Difference in mid-level clouds between 2014-2021 and 1983-2013; (g) High-level clouds for 1983-2013; (h) High-level clouds for 2014-2021; (i) Difference in high-level clouds between 2014-2021 and 1983-2013; (j) Total cloud cover for 1983-2013; (k) Total cloud cover for 2014-2021; (l) Difference in total cloud cover between 2014-2021 and 1983-2013.

3.6. SSTA, OLR and Horizontal Winds Anomalies

The analysis of sea surface temperature anomalies (SSTA), wind vectors (U/V), and outgoing longwave radiation (OLR) over the tropical Pacific during JJA, as depicted in Figure 8, elucidated the large-scale climate drivers contributing to Rwanda's pronounced JJA Tmin escalation around 2013, with impacts spanning global, regional, and local scales. From 1983 to 2013, Figure 8(a) showed a global SSTA pattern with moderate variability across the tropical Pacific, indicative of neutral ENSO conditions. Wind vectors reflected typical trade wind patterns with no significant anomalies, and OLR exhibited moderate cooling, suggesting balanced convection, with statistical significance at 95% Confidence Level marked by dots. Regionally, over East Africa, this period demonstrated stable atmospheric conditions with minimal influence on cloud cover or convection. In Rwanda, these neutral conditions contributed to a relatively stable radiative environment, with no notable impact on nighttime Tmin.

By 2014-2021, Figure 8(b) revealed a pronounced El Niño event globally, with warmer SSTA (up to +0.6˚C) in the central-eastern Pacific and cooler anomalies (−0.6˚C) in the western Pacific, alongside strengthened easterly wind vectors indicating an intensified Walker Circulation. Reduced OLR over East Africa signified enhanced convection, with significant changes (95% Confidence Level, dots) observed. Regionally, this shift increased moisture transport and convection over East Africa, reducing cloud cover and OLR further. In Rwanda, particularly in the eastern and central lowlands, these changes amplified radiative heating, with reduced cloud cover diminishing nighttime cooling, thus driving the sustained Tmin rise through 2021.

The difference map, Figure 8(c), confirmed these post-2013 shifts: a stronger El Niño signature, altered wind patterns, and intensified convection over East Africa, significantly impacting Rwanda by reducing nighttime cooling and elevating Tmin. These findings, validated at 95% Confidence Level, underscored the influence of ENSO-driven dynamics on Rwanda's temperature extremes, highlighting the eastern and central lowlands' vulnerability and the urgent need for targeted climate adaptation strategies and further research into global-regional teleconnections.

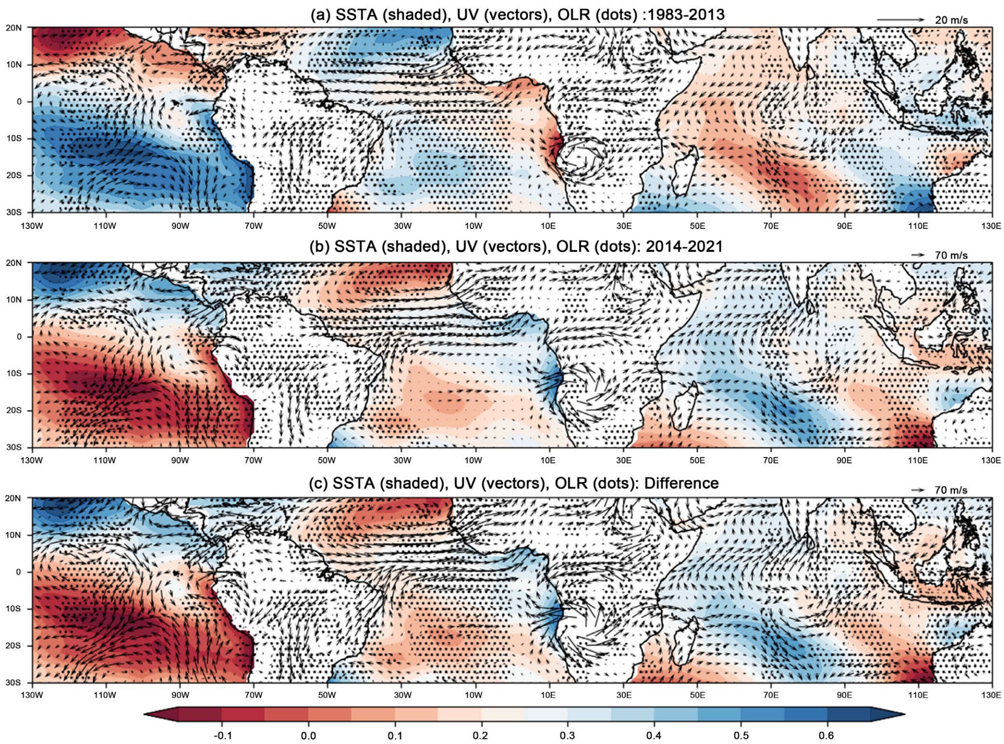

Figure 8. Sea surface temperature anomalies (shadings, ˚C, −0.6 to +0.6), U/V wind vectors (m/s, 20 m/s scale, and OLR anomalies during JJA, with 95% Confidence level indicated by dots representing statistical significance. (a) SSTA, U/V vectors), and OLR (dots) for 1983-2013; (b) SSTA, U/V vectors, and OLR (dots) for 2014-2021; (c) Difference in SSTA, U/V vectors, and OLR (dots) between 2014-2021 and 1983-2013.

4. Conclusion

The sharp rise in Tmin during JJA season of 2013 in Rwanda's eastern and central lowlands was sought to be unraveled in this study, with its ties to atmospheric circulation shifts from 1983 to 2021 analyzed. A persistent Tmin warming trend was confirmed through the results, with intensification observed post-2013, anomalies reaching +2.4˚C (e.g., Tmin elevated to 15.5˚C - 16.5˚C in Kigoma and Kiziguro), and increases in Tmax surpassed. The eastern and central lowlands were pinpointed as variability hotspots by EOF analysis. The 2013 anomaly was found to have been driven by a confluence of factors: enhanced upward motion, strengthened equatorward winds, elevated humidity, and a significant reduction in low-level, high-level, and total cloud cover, all deemed statistically significant at 95% confidence level, whereby daytime cooling was curtailed and nighttime radiative heating boosted. Amplification of these local dynamics was affected by large-scale forcing from ENSO, with the Walker Circulation strengthened, divergence over East Africa increased, and Pacific SSTA raised, whereby moisture transport and convection were driven higher, cloud cover and OLR further diminished. The critical interplay of regional atmospheric changes and global climate systems in triggering Rwanda's 2013 JJA Tmin spike was highlighted by these findings, with actionable insights provided for climate models to be enhanced and adaptation strategies tailored to safeguard the nation's agriculture and water resources amid rising temperature extremes. However, broader generalization is limited by the study's focus on a specific timeframe (1983-2021) and lowland regions, alongside the influence of upper-atmospheric factors like wind shear left unexamined. Spatial and temporal analyses could be extended, or additional variables could be incorporated in future research to refine forecasting accuracy. As Rwanda is confronted with a warming climate, with JJA Tmin anomalies threatening its climate-sensitive economy, the pressing need to understand such events better to strengthen resilience, particularly for vulnerable agricultural communities, is emphasized by this work.

Acknowledgements

The first author appreciates acknowledging the Government of RWANDA for providing an opportunity to carry on with studies and the Ministry of Commerce of China (MOFCOM) for sponsorship. Many thanks to Prof. TAN GUIRONG for supervising and guiding this research. Many thanks to ECMWF-ERA5, NOAA and Rwanda Meteorology Agency for data availability.

Conflicts of Interest

The authors declare no conflicts of interest regarding the publication of this paper.

References

[1] Nury, A.H., Hasan, K., Alam, M.J.B. and Hasan, M.M. (2017) Analysis of Time Series Variations of Temperature and Its Forecast in the Northeastern Bangladesh. *Interna-*

tional Journal of Global Warming, **13**, 157-182. https://doi.org/10.1504/ijgw.2017.086283

[2] Kouassi, A.M., Gnangouin, A.Y.J., Abdoul-Karim, N.R. and Khadara, D. (2022) Impacts of Climate Change on Agroclimatic Indicators in West Africa: Case Study of the N'zi (Bandama) Watershed in Côte d'Ivoire. *Current Journal of Applied Science and Technology*, **41**, 35-48. https://doi.org/10.9734/cjast/2022/v41i434006

[3] Intergovernmental Panel on Climate Change (IPCC) (2023) Annex I: Observational Products. In: *Climate Change* 2021—*The Physical Science Basis*: *Working Group I Contribution to the Sixth Assessment Report of the Intergovernmental Panel on Climate Change*, Cambridge University Press, 2061-2086.

[4] Safari, B. and Sebaziga, J.N. (2023) Trends and Variability in Temperature and Related Extreme Indices in Rwanda during the Past Four Decades. *Atmosphere*, **14**, Article 1449. https://doi.org/10.3390/atmos14091449

[5] Ngarukiyimana, J.P., Fu, Y., Sindikubwabo, C., Nkurunziza, I.F., Ogou, F.K., Vuguziga, F., *et al*. (2021) Climate Change in Rwanda: The Observed Changes in Daily Maximum and Minimum Surface Air Temperatures during 1961-2014. *Frontiers in Earth Science*, **9**, Article 619512. https://doi.org/10.3389/feart.2021.619512

[6] Karl, T.R., Jones, P.D. and Kukla, G. (2015) Asymmetric Trends of Daily Maximum and Minimum Temperature. Papers in Natural Resources.

[7] Rwanda Meteorology Agency (2022) Downscaled Climate Projections for National Adaptation Plan in Rwanda. 14. https://www.rema.gov.rw

[8] Muhumure, J., Pohl, E. and Schulz, S. (2024) Assessing the Impact of Climate Change on Spring Discharge Using Hydrological Modelling in Musanze District, Rwanda. *Hydrogeology Journal*, **32**, 1909-1923. https://doi.org/10.1007/s10040-024-02836-5

[9] Safari, B. (2012) Trend Analysis of the Mean Annual Temperature in Rwanda during the Last Fifty Two Years. *Journal of Environmental Protection*, **3**, 538-551. https://doi.org/10.4236/jep.2012.36065

[10] Seshaba, P., Singirankabo, E. and Nsabimana, D. (2024) Analysis of Extreme Temperature Variability in Rwanda. *Journal of Atmospheric Science Research*, **7**, 74-89. https://doi.org/10.30564/jasr.v7i1.6107

[11] Buheji, M., Mushimiyimana, E. and Kwizera, A. (2024) Adapting to Change: Understanding Rwanda's Socioeconomic Resilience in the Face of Climate Variability. *Resources and Environment*, **14**, 51-59.

[12] Jonah, K., Wen, W., Shahid, S., Ali, M.A., Bilal, M., Habtemicheal, B.A., *et al*. (2021) Spatiotemporal Variability of Rainfall Trends and Influencing Factors in Rwanda. *Journal of Atmospheric and Solar-Terrestrial Physics*, **219**, Article ID: 105631. https://doi.org/10.1016/j.jastp.2021.105631

[13] Sebaziga, J.N., Twahirwa, A., Kazora, J., Rusanganwa, F., Mbati, M.M., Higiro, S., *et al*. (2023) Spatial and Temporal Analysis of Rainfall Variability and Trends for Improved Climate Risk Management in Kayonza District, Eastern Rwanda. *Advances in Meteorology*, **2023**, Article ID: 5372701. https://doi.org/10.1155/2023/5372701

[14] Siebert, A., Dinku, T., Vuguziga, F., Twahirwa, A., Kagabo, D.M., delCorral, J., *et al*. (2019) Evaluation of Enacts-Rwanda: A New Multi-Decade, High-Resolution Rainfall and Temperature Data Set—Climatology. *International Journal of Climatology*, **39**, 3104-3120. https://doi.org/10.1002/joc.6010

[15] Kazapua, I.T., Yu, Y., Hu, M. and Liu, J. (2024) Spatial and Temporal Variability of Solar Irradiance in Botswana. *Journal of Geoscience and Environment Protection*, **12**, 221-251. https://doi.org/10.4236/gep.2024.1211013

[16] Singirankabo, E., Iyamuremye, E., Habineza, A. and Nelson, Y. (2023) Statistical Modelling of Maximum Temperature in Rwanda Using Extreme Value Analysis. *Open Journal of Mathematical Sciences*, **7**, 180-195. https://doi.org/10.30538/oms2023.0206

[17] Chakraborty, D., Saha, S., Singh, R.K., Sethy, B.K., Kumar, A., Saikia, U.S., *et al.* (2017) Trend Analysis and Change Point Detection of Mean Air Temperature: A Spatio-Temporal Perspective of North-Eastern India. *Environmental Processes*, **4**, 937-957. https://doi.org/10.1007/s40710-017-0263-6

[18] Ndulue, E.L. and Mbajiorgu, C.C. (2018) Modeling Climate and Land Use Change Impacts on Streamflow and Sediment Yield of an Agricultural Watershed Using SWAT. *Agricultural Engineering International*, **20**, 15-25.

[19] Ayugi, B., Tan, G., Niu, R., Dong, Z., Ojara, M., Mumo, L., *et al.* (2020) Evaluation of Meteorological Drought and Flood Scenarios over Kenya, East Africa. *Atmosphere*, **11**, Article 307. https://doi.org/10.3390/atmos11030307

[20] Ayugi, B., Shilenje, Z.W., Babaousmail, H., Lim Kam Sian, K.T.C., Mumo, R., Dike, V.N., *et al.* (2022) Projected Changes in Meteorological Drought over East Africa Inferred from Bias-Adjusted CMIP6 Models. *Natural Hazards*, **113**, 1151-1176. https://doi.org/10.1007/s11069-022-05341-8

[21] Mbawala, J.R., Li, H., Zeng, J., Ndabagenga, D.M., Tan, A., Beukes, D.J., *et al.* (2024) Analysis of Changes of Extreme Temperature during June to August Season over Tanzania. *Journal of Geoscience and Environment Protection*, **12**, 44-56. https://doi.org/10.4236/gep.2024.122003

[22] King'uza, P. and Tilwebwa, S. (2019) Inter-annual Variability of March to May Rainfall over Tanzania and Its Association with Atmospheric Circulation Anomalies. *Geographica Pannonica*, **23**, 147-161. https://doi.org/10.5937/gp23-22430

[23] Manatsa, D., Chingombe, W. and Matarira, C.H. (2008) The Impact of the Positive Indian Ocean Dipole on Zimbabwe Droughts. *International Journal of Climatology*, **28**, 2011-2029. https://doi.org/10.1002/joc.1695